IEEE Access
Multidisciplinary | Rapid Review | Open Access Journal

Received September 3, 2019, accepted September 16, 2019, date of publication September 19, 2019,
date of current version October 3, 2019.

Digital Object Identifier 10.1109/ACCESS.2019.2942318

Crack Junction Detection in Pavement Image Using Correlation Structure Analysis and Iterative Tensor Voting

YANLI WANG[1], YUCHUN HUANG[2], AND WEIHONG HUANG[3]
[1]State Key Laboratory of Information Engineering in Surveying, Mapping, and Remote Sensing (LIESMARS), Wuhan University, Wuhan 430079, China
[2]School of Remote Sensing and Information Engineering, Wuhan University, Wuhan 430079, China
[3]Chongqing Communications Planning Survey and Design Institute, Chongqing 400067, China

Corresponding author: Yuchun Huang (hycwhu@whu.edu.cn)

This work was supported in part by the Natural Science Foundation of China under Project 41671419 and Project 51208392, in part by the High-tech program of Chongqing under Grant cstc2018jszx-cyzdX0134, in part by the Collaborative Innovation Center of Geospatial Technology, and in part by the Fundamental Research Funds for the Central Universities under Grant 2042017KF0235.

ABSTRACT Crack junction is the crossing or branching point of different cracks in the pavement image. It represents the branch of transverse crack or longitudinal crack, and describes the interlaced network of alligator crack. It is a simple yet important factor to characterize the type and severity level of crack. This paper is motivated to robustly detect crack junctions of any type and size in pavement image, regardless of the pavement interferences. In this paper, the contrast between the crack junction and pavement background is first enhanced by removing the large interferences and background. Then, based on the structure characteristic of crack curves, correlation structure index is proposed to locate candidates of crack junctions. Actual junctions are extracted among the candidates with the unified ball tensor structure after the iterative tensor voting. The proposed method is tested with the concrete pavement images of public data set of SDNET2018 and asphalt pavement images collected by the unmanned aerial vehicle on the highway G45 in China. Experimental results demonstrate that the proposed method can detect crack junctions with the correctness of 0.891 and completeness of 0.887. It can be applied to junction detection on concrete and alligator pavement with different noise and interference, and is promising to classify the crack type and quantify the severity level.

INDEX TERMS Crack junction, correlation structure analysis, iterative tensor voting, structure characterization.

I. INTRODUCTION

After the vast investment into the construction of transportation infrastructure, the post-construction maintenance has become a crucial problem for transportation agencies around the world. Due to meteorological weathering, constant overloading, sub-base failure, poor drainage, etc., pavement condition deteriorates greatly with such distresses as cracking, rutting, pothole. To prevent these distresses causing passenger injury and economic loss, pavement condition survey is conducted regularly to make a timely and appropriate treatment for the road maintenance. Among these pavement distresses, crack is one of the most common and harmful distresses. Traditionally, the pavement crack condition is investigated manually. It is dangerous, costly, time consuming, and labor intensive [1], [2]. With the rapid development of unmanned aerial vehicles (UAV) and mobile sensing vehicles, it is convenient to obtain high-resolution optical pavement images. Pavement crack condition can be analyzed at the office computer using the collected images, which saves a large amount of human and material resources.

As seen in Figure 1, crack junction is the crossing or branching point of different cracks of the pavement image. It represents the branch of transverse crack or longitudinal crack. The interlaced network of alligator crack is decided by junctions. Also, the number and distribution of crack junctions tell the great details of the crack type, extent, and severity level. Crack junction also indicates the type and

The associate editor coordinating the review of this manuscript and approving it for publication was Utku Kose.

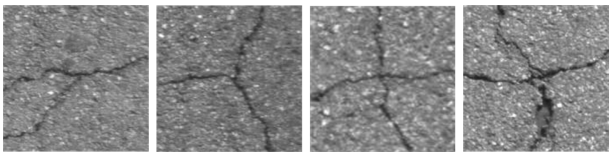

FIGURE 1. Examples of the crack junction.

severity level change of pavement crack, which is adopted and implemented in some protocols for crack classification and severity level quantification [3]–[9]. They are simple yet important factor to classify the crack and plays an important role in reflecting the severity of pavement cracks, especially for the alligator crack.

However, currently, there is a little literature dedicated to the study of crack junction. Many researchers are focusing on crack detection and classification with pavement images. Some methods of crack detection and classification are based on crack topology and a priori knowledge [10]–[12]. Ghanta et al. adopted the Hessian matrix to extract crack direction and classified pavement cracks into three types based on the direction and the area covered [13]. Arena et al. focused on crack quantification by crack topology, such as the orientation, length, width and aspect ratio of the cracks, which were important to analyze the type and severity of cracks [14]. Based on genetic programming and percolation model, Qu et al, presented a robust and effective genetic algorithm to detect real concrete surface cracks [15]. As the key points of crack structures, Jiang extracted crack junctions through iterative morphological thinning and skeleton analysis and then detect the continuous crack curves between these key points using the minimal path method [16]. On the other hand, some researchers employed deep learning methods to detect cracks automatically [17]–[21]. Cha et al. used the convolutional neural networks (CNN) to identify the concrete cracks from images. The proposed CNN method showed robust performance compared to the traditional edge detection methods (i.e., Canny and Sobel) in the complex background [22]. Yang et al. applied fully convolutional network to identify and measure diverse cracks concurrently at pixel level, which performed robustly under different imaging conditions [23]. Other learning methods, such as support vector machine, AdaBoost, or recurrent neural network [24]–[26], also performed well for crack detection and classification. However, for the machine learning method, a large number of crack samples are collected manually to ensure the detection precision, which is costly and tedious. In the pavement images, the crack is surrounded by more noise and different interferences and affected by the camera focus fuzzy and image illumination unevenly. Therefore, the robust crack detection method is still the focus of research.

In other related areas, the importance of junctions has received great attention. Junctions have provided important cues in computer vision and image-understanding tasks, such as stereo matching, indoor localization, writer identification, disease diagnosis and change detection [27]–[30]. Junction detection methods can be classified into three categories: corner-based, contour-based, and template-based [31]. Luo et al. employed the Harris corner detector to extract junction [32]. Meanwhile, some researchers detected junctions using the edge map [33]–[35]. Based on the vessel centerline, Abbasi et al., applied the geometrical and topological properties of the blood vessels passing through junction candidates to identify the true junction from the other structures [36]. Moreover, lots of researchers dedicated themselves to detect junction by a generic template. Based on the combined information of Hessian and correlation matrix, Su et al., extracted junction candidates first, and then adopted a Gaussian-shaped multi-scale stick template to validate the candidates [37]. Sinzinger first extracted junction candidates by a preliminary corner detector and then refined those candidates by an affine invariant junction template [38]. Xia et al. proposed a junction template that can set the detection parameter automatically and keep the contrast invariant [39]. Therefore, the crack junction is an important factor to extract the semantic structure of pavement cracks and indicates the type and severity level change of pavement crack.

Although many methods of junction detection have been developed in the related areas, real pavement images have complex lighting conditions and various interferences. Therefore, there are still many challenges with the crack junction detection in the pavement image, such as:

- Due to fuzzy focus and insufficient illumination around some crack junction, the boundary between hair-line crack and pavement surface becomes blurry and noisy. The crack junction formed by crossing hair-line cracks is unobvious. Additionally, for crack junctions with different type, size and intensity contrast, it is difficult to detect them all by a simple and uniform template.
- There are lots of interferences in the pavement image, such as shadow, dirt debris, lane marking, which could happen around the crack junction. Different interferences have different shape and intensity. Junction-like structures near the edge of these interferences could mislead the crack junction detection with the traditional edge detectors.

This paper is motivated to robustly detect crack junctions in pavement image, regardless of their type and size. Before crack junction detection, a pavement image enhancement method is applied to enhance the contrast between the crack junction and the background by removing large interferences and the background. Based on the characteristic of gradient of the enhanced crack edges, the correlation structure analysis is employed to characterize the crack structure. Then, the candidates of crack junctions are located using the proposed correlation structure index. Unlike the traditional corner- or template-based methods, actual junctions are extracted from the candidates with the unified ball tensor structure after the iterative tensor voting. The whole framework of our method can be composed of three parts: pavement image enhancement, crack structure characterization, and crack junction detection, as shown in Figure 2.

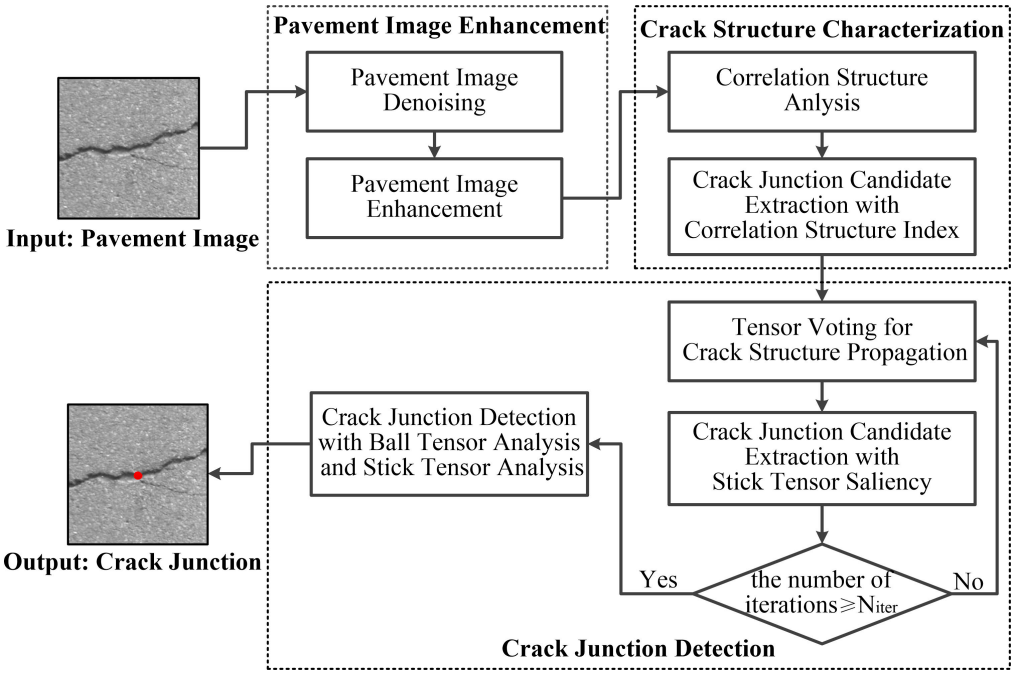

FIGURE 2. Flowchart of the proposed method for crack junction detection.

The remainder of this paper is organized as follows: Section II presents the proposed method for crack junction detection. Section III shows the experimental results. Section IV discuss the parameter setting in our method. Conclusions are drawn in Section V.

II. METHODOLOGY

A. PAVEMENT IMAGE ENHANCEMENT

Pavement image is full of noise due to different texture of pavement materials, imaging condition, etc. It blurs the contrast near the edge of pavement crack. Also, there are many large interferences, such as lane marking, shadow, etc. If crack curves cross these large interferences, junction-like structures will be formed at the intersection of the crack and the edges of these interferences and may be mistakenly extracted as pavement crack junction. Hence, it is necessary to enhance the pavement image by denoising and removing large interferences before crack junction detection.

1) PAVEMENT IMAGE DENOISING

To remove noises to some extent and keep the crack edges from being blurred, bilateral filtering is employed here. The bilateral filter is composed of two filter kernels: a spatial filter kernel $c(p, q)$ that measures the geometric closeness and a range filter kernel $s(I_p, I_q)$ that measures the intensity similarity [40]. It can be calculated by the following equation:

$$I_p^B = \omega_p^{-1} \sum_{q \in \Omega_p} c(p, q) \times s(I_p, I_q) \times I_q \tag{1}$$

where $\omega_p = \sum_{q \in \Omega} c(p, q) \times s(I_p, I_q)$ is the normalizing parameter. I_p is the current gray-level of pixel p. I_p^B is the result of bilateral filtering. Ω_p is the filtering region of pixel p. $c(p, q)$ and $s(I_p, I_q)$ are usually calculated by Gaussian kernel in practice.

$$c(p, q) = exp(-\frac{d^2(p, q)}{2\sigma_d^2}) \tag{2}$$

$$s(I_p, I_q) = exp(-\frac{|I_p - I_q|^2}{2\sigma_r^2}) \tag{3}$$

where $d(p, q)$ is the distance between p and q. σ_d, σ_r are the parameters controlling the effective support of $c(p, q)$ and $s(I_p, I_q)$, respectively. It can be seen that if pixel q is closer to pixel p and the gray-level of pixel q is more similar to that of pixel p, I_q will have a greater effect on I_p^B.

In the pavement image, the noises are removed effectively, while cracks are kept clearly owing to the obvious intensity difference between crack edges and pavement and the suppressing effect of $s(I_p, I_q)$, as shown in Figure 3.

2) PAVEMENT IMAGE ENHANCEMENT

To discard the large interferences and the useless pavement background from the bilateral-filtered image, median

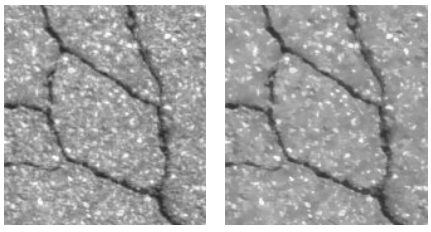

(a) (b)

FIGURE 3. Result of pavement image denoising. (a) Original image, (b) bilateral-filtered image.

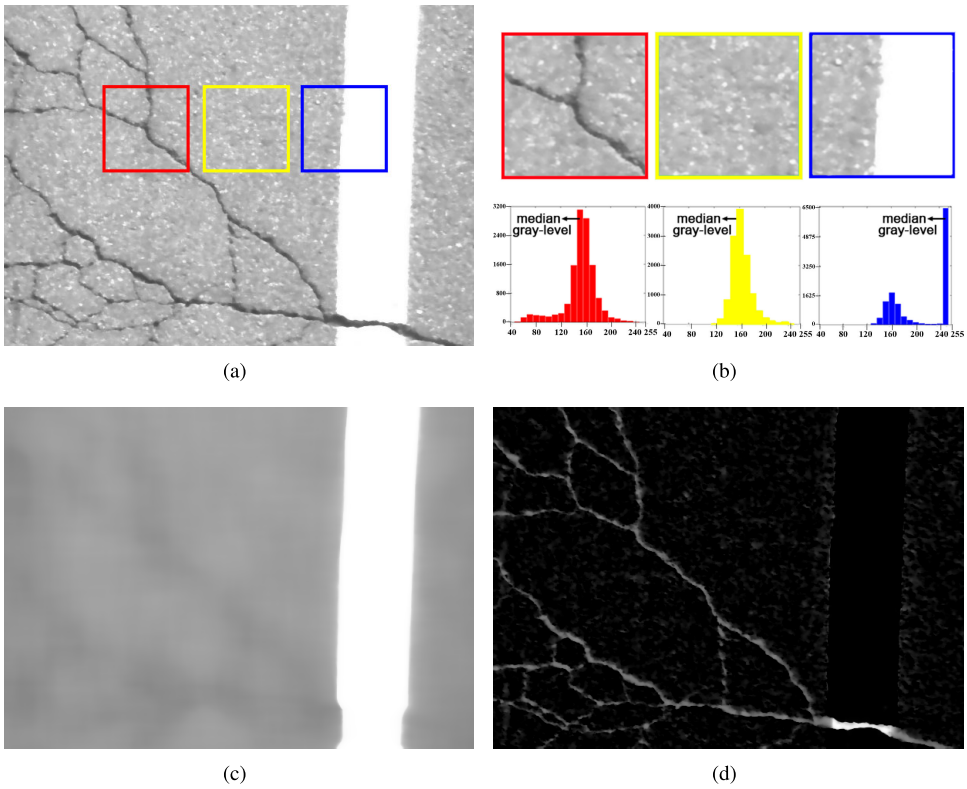

FIGURE 4. Pavement image enhancement. (a) Bilateral-filtered image, (b) gray-level histograms of three structures, (c) result of median filtering with large window, (d) result of pavement image enhancement.

filtering with large window is employed to enhance crack junction. Median filter is a kind of statistical order filter, and finds the median gray-level of the filtering window Ω_p [41]. It can be calculated by the following equation:

$$I_p^M = med\{I_q^B, q \in \Omega_p\} \tag{4}$$

where I_p^M is the result of median filtering. I_q^B is the result of bilateral filtering.

As shown in the histograms of Figure 4(b), for crack, small stone mixture and lane marking, the median gray-levels in the large local patch correspond to the gray-level of pavement, pavement and lane markings, respectively. Then, the pavement background and lane marking are extracted correctly by the median filtering with large window as shown in Figure 4(c). As shown in Figure 4(d), the pavement image is enhanced by subtracting the median-filtered image from the bilateral-filtered image. The large interferences and useless pavement background are removed. The contrast between the crack junction and background is improved significantly.

B. CRACK STRUCTURE CHARACTERIZATION

Crack junction is the special structure of cracks in pavement image. Pixels of the crack curves are recognized as crack junction candidates in our method. After pavement image enhancement, there remains lots of aggregate of stone mixtures of arbitrary sizes and positions in the asphalt pavement image. It is difficult to differentiate the aggregate and crack pixels from the intensity contrast perspective owing to the similar intensity change around the crack and the stone mixture after the enhancement. But, in the view of structure, crack has a linear structure while stone mixture is a point-like structure in a local patch. This structure characteristic is generic and robust to different imaging conditions, such as over- or under-exposed lightening conditions.

As shown in Figure 5(a), gradients of cracking edges are perpendicular to the crack direction locally. Most of the crack gradients have similar direction and stronger gradient magnitude in their local patch. The projection of gradients of all crack edge pixels along the crack direction is small in the local patch. In contrast, the projection along the orthogonal direction of crack is far larger. For stone mixtures, the directions of stone mixture gradients are anisotropic and vary a lot in Figure 5(b). Therefore, the gradient projections along

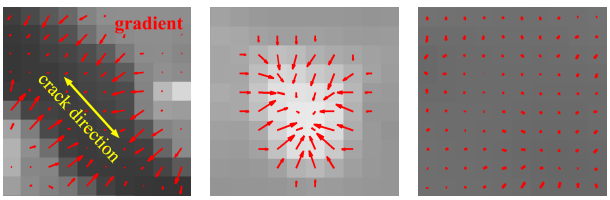

FIGURE 5. Gradients of different structures in the pavement image. (a) Crack, (b) stone mixture, (c) pavement.

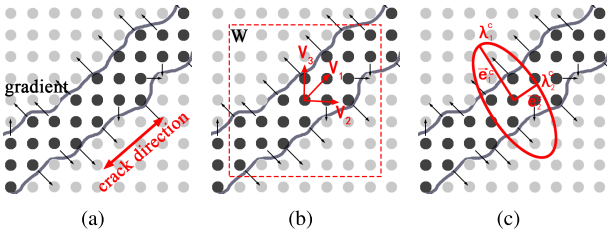

FIGURE 6. Correlation structure analysis of crack. (a) Gradients of crack edges, (b) projection direction $\vec{v}_i$ in the local patch W, (c) result of correlation structure analysis.

all directions are almost identical. For pavement pixels in Figure 5(c), due to the invariant pavement texture, gradients are very low and gradient projection is relatively quite small. Therefore, based on the gradient projection differences, crack junction candidates can be extracted. Correlation structure analysis is adopted here to obtain these gradient projection differences.

1) CORRELATION STRUCTURE ANALYSIS

As shown in Figure 6(b), there are $N \times N$ pixels in the local patch W. The gradient of each pixel is represented as $\vec{g}$. And the gradient set of W is represented as $G = \{\vec{g}_i\}_{i=1}^{m_w}$. m_w is the number of the pixels in W. Since local crack direction $\vec{v}$ is perpendicular to the gradients of cracking edges, it can be obtained by minimizing the projection of all the gradients along $\vec{v}$ in W. The projection of all the gradients along $\vec{v}$ is calculated by the following equation:

$$E(V) = \frac{1}{m_w}\sum_{i=1}^{m_w}(\vec{g_i}^T\vec{v})^2 = \vec{v}^T(\frac{1}{m_w}\sum_{i=1}^{m_w}(\vec{g_i}\vec{g_i}^T)\vec{v} \tag{5}$$

Let $G = \frac{1}{\sqrt{m_w}}[\vec{g}_1, \vec{g}_2, ..., \vec{g}_n]$

The equation 5 can also be expressed as:

$$E(V) = \vec{v}^T GG^T\vec{v} \tag{6}$$

Then, the minimal projection can be obtained by the first-order derivative of E(v) with respect to the unit length $\vec{v}$ [42].

$$\nabla E(V) = 2GG^T\vec{v} = 0 \tag{7}$$

Let $M' = GG^T$ be the correlation matrix and can be calculated as follows:

$$M' = \frac{1}{m_w}\sum_{i=1}^{m_w}(\vec{g_i}\vec{g_i}^T) = \frac{1}{n^2}\sum_{i=1}^{n^2}\begin{bmatrix} g_{ix}^2 & g_{ix}g_{iy} \\ g_{ix}g_{iy} & g_{iy}^2 \end{bmatrix} \tag{8}$$

where g_{ix}, g_{iy} are the gradient value along x direction and y direction, respectively.

Let $\lambda_1^c, \lambda_2^c(\lambda_1^c \geq \lambda_2^c)$ be the eigenvalues of correlation matrix M', $\vec{e_1}^c, \vec{e_2}^c$ be the corresponding eigenvectors. The minimal projection of $E(v)$ happens along $\vec{e_2}^c$. The local crack direction is then decided by $\vec{e_2}^c$. λ_1^c, λ_2^c denote the gradients projections along the crack direction and the orthogonal direction of crack respectively as shown in Figure 6(c).

Different structures in the pavement image can be characterized by the gradient projection differences after correlation structure analysis as shown in Figure 7. For the crack, λ_1^c is far greater than λ_2^c in Figure 7(a). Nevertheless, λ_1^c, λ_2^c of stone mixture are close in Figure 7(b). For the pavement, both λ_1^c and λ_2^c are very small in Figure 7(c).

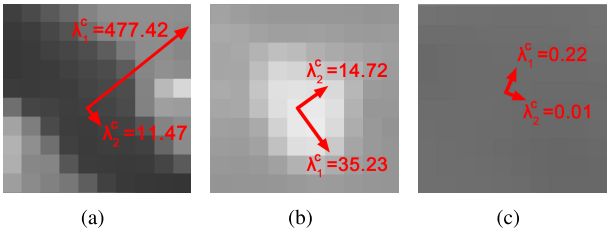

FIGURE 7. Structure characterization of different structures in the pavement image by correlation structure analysis. (a) Crack, (b) stone mixture, (c) pavement.

2) CORRELATION STRUCTURE INDEX OF CRACK

Base on the gradient projection differences after correlation structure analysis, a correlation structure index is proposed to characterize these differences from the structure perspective and differentiates the crack-like structure from the other point-like structure. The correlation structure index of crack P_{crack} is defined as the biased ratio of the gradient projections along the crack direction and the orthogonal direction of crack, i.e.,

$$P_{crack} = \frac{\lambda_1^c}{\lambda_2^c + mean(\lambda_1^c)} \tag{9}$$

where λ_1^c and λ_2^c denote the gradient projections along the crack direction and the orthogonal direction respectively. The offset item mean λ_1^c is adaptively set as the mean of λ_1^c of all local patches in the pavement image. It insures the reliability of P_{crack} in case of infinitesimal λ_2 and detect the crack junction candidates under various image conditions.

To obtain the appropriate threshold for crack junction candidate extraction, some samples of pavement, stone mixture, dirt debris and crack, are collected to analyze the characteristic of correlation structure index for different structures. As shown in Figure 8, the correlation structure index of crack is usually higher than 10 with the high probability

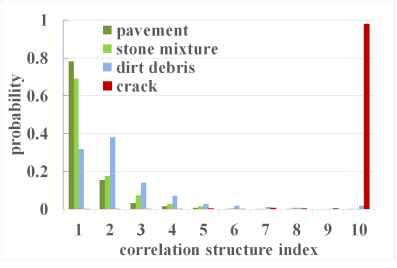

FIGURE 8. Histogram of correlation structure index of different structures.

of 0.97. However, correlation structure indexes of other structures mainly distribute from 0 to 4. Therefore, based on this index, crack junction candidates can be easily extracted by thresholding.

C. CRACK JUNCTION DETECTION

Although crack junctions have different type, size and intensity, there is a common characteristic: the crack junction is like a ball and has no obvious direction. Hence, the ball-like structure characterization of ball tensor is adopted in this paper for the crack junction detection. Furthermore, as shown in Figure 9, there are some breaking segments on the crack curves owing to the physical breakup of faint crack, imaging condition or incorrect threshold of crack structure. The crack junctions can not be detected when gap of breaking segments appears near them. Therefore, iterative tensor voting is employed for crack junction candidates to propagate their crack-like structure in the neighborhood and link the breaking segments naturally. After iterations, based on the characteristic of ball tensor, candidates of crack junction are validated to extract the crack junction accurately.

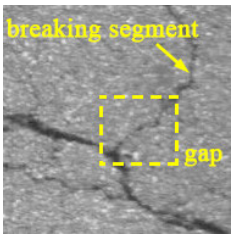

FIGURE 9. An illustration of breaking segment on crack curves.

1) TENSOR CHARACTERIZATION OF CRACK JUNCTION

In pavement image, the symmetric, non-negative definite, second-order tensor T is a 2×2 matrix. It characterizes the optimal directions and the structure saliencies of perceptual structure as the following equation [43].

$$T = \lambda_1 \vec{e_1} \vec{e_1}^T + \lambda_2 \vec{e_2} \vec{e_2}^T \tag{10}$$

where $\lambda_1, \lambda_2 (\lambda_1 \geq \lambda_2)$ are the eigenvalues of T. $\vec{e_1}, \vec{e_2}$ are the corresponding eigenvectors. From the view of structure, $\vec{e_1}$ and $\vec{e_2}$ represent the normal and tangnet orientations of the structure respectively. T can be further decomposed as follows:

$$T = (\lambda_1 - \lambda_2) \vec{e_1} \vec{e_1}^T + \lambda_2 (\vec{e_1} \vec{e_1}^T + \vec{e_2} \vec{e_2}^T) \tag{11}$$

The first term is named stick tensor, and the coefficient $(\lambda_1 - \lambda_2)$ is the saliency of stick tensor that indicates the probability of being a curve. The second term is ball tensor, and λ_2 is the saliency of ball tensor that indicates the probability of being a ball structure. If the saliency is large, the structure possibility is high.

To characterize tensor vividly, T can also be viewed as an ellipse, which $\vec{e_1}, \vec{e_2}$ are the orientations of ellipse and λ_1, λ_2 are the length of the semi-axes as shown in Figure 10. When λ_1 is much larger than λ_2, T can be seen as a flat ellipse in Figure 10(a). It means there is an optimal orientation and is the same as the structure of crack curves. Thus, $\lambda_1 - \lambda_2$ indicates the probability of being crack curves in the pavement image. If λ_1 is similar to λ_2, T is like a ball and equal to its ball tensor in Figure 10(b). The ball tensor has no optimal direction and is similar to the structure of crack junctions. Hence, in pavement image, the stick tensor and ball tensor can be used to represent the crack curves and crack junction, respectively, as illustrated in Table 1. The ball tensor can be used to uniformly characterize the crack junction of different size, type, intensity or formed by crack curve with different orientations.

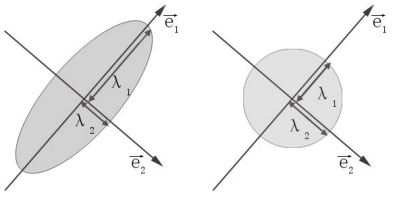

FIGURE 10. Ellipse characterization of tensor. (a) Stick tensor (crack curve), (b) ball tensor (crack junction).

TABLE 1. Tensor characterization of different structures in pavement image.

structure	tensor characterization	saliency	orientation
crack	stick tensor	$\lambda_1 - \lambda_2$	normal: $\vec{e_1}$
crack junction	ball tensor	λ_2	none
pavement	NA	low λ_1, λ_2	NA

2) ITERATIVE TENSOR VOTING

To obtain the accurate tensor structure information of candidates, tensor voting is applied. Tensor voting is a mechanism, which adopts tensor-based structure characterization and propagates structure indication to the neighbors in a voting manner. As seen in Figure 11(a), a unit length stick tensor N is located at P and the orientation of N is perpendicular to the x-axis. To propagate the structure indication in a smooth path, the osculating circle O of N is adopted to propagate structure from P to Q, which maintains the constant

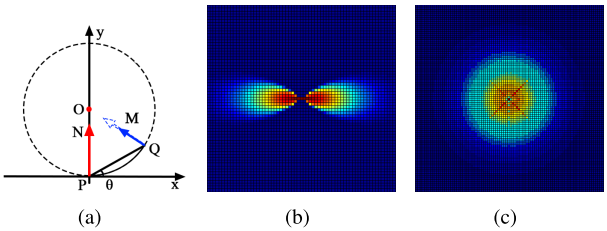

FIGURE 11. Tensor voting and tensor field. (a) Tensor voting of the unity stick tensor (b) Stick tensor field, (c) ball tensor field.

curvature [44]. The orientation of structure M propagated by N is lying along the radius of O. Based on the distance and curvature, the saliency of structure indication is decided by the saliency decay function as the following equation:

$$DF(s,k,\sigma) = e^{-\frac{s^2+ck^2}{\sigma^2}} \tag{12}$$

where s is the length of the arc from P to Q, k is the curvature of the arc. σ is the scale parameter of tensor voting and controls the size of voting field Wsize as seen in equation 13.

$$Wsize = \lfloor \frac{\lceil 2 \times \sqrt{-log(0.01) \times \sigma^2} \rceil}{2} \rfloor \times 2 + 1 \tag{13}$$

c is a constant related with σ, $c = \frac{-16log(0.1)\times(\sigma-1)}{\pi^2}$, and controls the decay degree of the curvature. It is optimized to make the extension of two orthogonal line segments to form a right angle equally likely to the completion of the contour with a rounded corner [43], [45]. Therefore, σ is the unique parameter in tensor voting and can be set according to the size of Wsize for actual demand. If the angle θ between the line PQ and the x-axis is larger than 45°, Q accepts no structure indication from P to avoid the false structure propagation. Finally, the structure indication M can be characterized as a tensor using the orientation and the saliency propagated by N as follows.

$$V_{stick} = DF(s,k,\sigma)e^{-\frac{s^2+ck^2}{\sigma^2}} \times \begin{bmatrix} -sin(2\theta) \\ cos(2\theta) \end{bmatrix} \begin{bmatrix} -sin(2\theta) & cos(2\theta) \end{bmatrix} \tag{14}$$

The stick tensor N of Figure 11(a) will propagate its structure indication of orientation and saliency in the voting field of Figure 11(b), where different color means different saliency. If N is a stick tensor with saliency $\lambda_1 - \lambda_2$, the propagated structure is characterized by product of V_{stick} and $\lambda_1 - \lambda_2$. The ball tensor can be seen as a summation of stick tensors that span the field of all possible orientation as the following equation:

$$V_{ball} = \int_0^{2\pi} RV_{stick}R^T d\theta' \tag{15}$$

where θ' is the direction where the stick tensor located. R is the rotation matrix to align V_{stick} with θ'. The voting field of ball tensor is illustrated in Figure 11(c).

To link the breaking segments naturally and obtain the tensor structure of candidates, the iterative tensor voting for crack structure propagation is applied in this paper. The whole process of tensor voting is composed of two parts: spare voting with ball tensor and dense voting with stick tensor as seen in Figure 12 [46]. First, the crack junction candidates of Figure 12(a) are encoded as a unit length ball tensor. Secondly, the crack structure is propagated between candidates by sparse voting with the ball tensor field of Figure 12(b). Each crack junction candidate accumulates the tensor structure characterization from their neighboring candidates. Initial crack direction and saliency of candidates are derived from the tensor accumulation and then encoded as stick tensor. Then, the dense voting with stick tensor field propagates the structure to all pixels in their voting field as shown in Figure 12(c). After structure propagation, the gap between breaking segments and crack junctions can also get the accurate structure indication propagated by the neighbors. Finally, cracks are characterized by the stick tensor and crack junctions are characterized by the ball tensor as shown in Figure 12(d). After tensor voting, some breaking segments cannot yet be connected well due to the small voting field. If we increase the size of the voting field, original structure of crack curves may be altered slightly. Using the iteration of small-field voting, breaking segments can be progressively linked to the crack junctions with no compromising of the crack structure. Moreover, stone mixture and dirt debris in the set of crack junction candidates are weakened due to the less indications of structure in the neighborhood after tensor. With iterations, these mixture and dirt debris will gradually disappear. Therefore, iterative tensor voting is adopted to enhance the structure of crack junction candidates and eliminate stone mixture and dirt debris. After current tensor voting, another iteration starts with the new crack junction candidates extracted by the stick tensor saliency, which include less small interferences, like large stone mixture, and more crack junctions until the number of iteration meets the given stopping conditions N_{iter}.

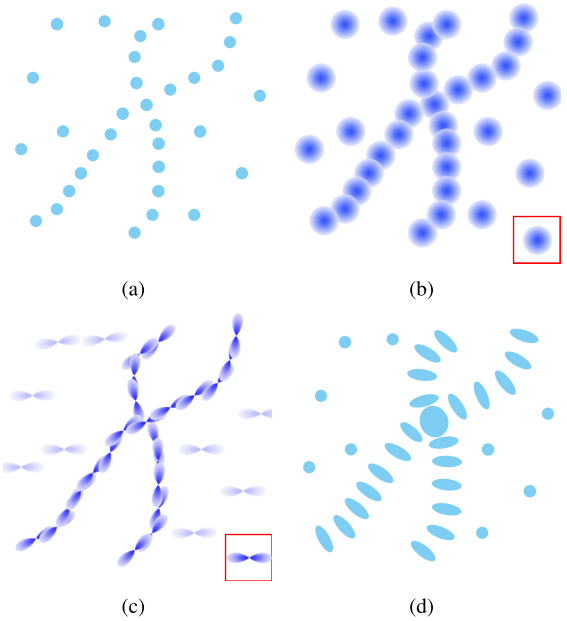

FIGURE 12. Iterative tensor voting for crack structure propagation. (a) Original crack junction candidate, (b) sparse voting with ball tensor field, (c) dense voting with stick tensor field, (d) tensor structure characterization.

3) CRACK JUNCTION DETECTION

After iterative tensor voting, the ball tensor saliency indicates the probability of being a crack junction. To extract the crack junction with different sizes, the local maximum of ball tensor saliency is applied as shown in Figure 13. Crack

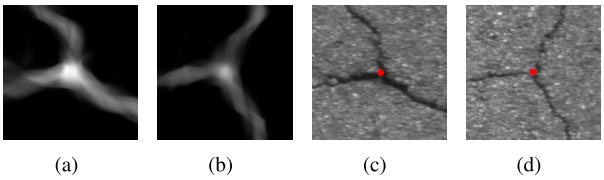

FIGURE 13. Crack junction detection for different size. (a-b) Ball tensor saliency, (c-d) Results of crack junction detection.

turn of Figure 14(a) is the special point of a crack curve, where the local crack direction turns significantly. The ball tensor saliency of crack turns is larger than the local pixels owing to the intersection of two orientations. They may be mistakenly extracted as crack junctions. However, there is a great structure difference between the crack turn and the crack junction. There are at least three linear structures around the crack junction while the crack turn is surrounded by only two linear structures. Hence, the number of peaks of stick tensor saliency is adopted to describe the number of linear structures around crack junction and eliminate the crack turns. Firstly, around the crack junction, a circle is drawn as shown in Figure 14(a) and 14(d). Then, the values of stick tensor saliency on the circle are recorded orderly. Finally, the crack junction is validated by analyzing the number of stick tensor peaks as shown in Figure 14(c) and 14(d).

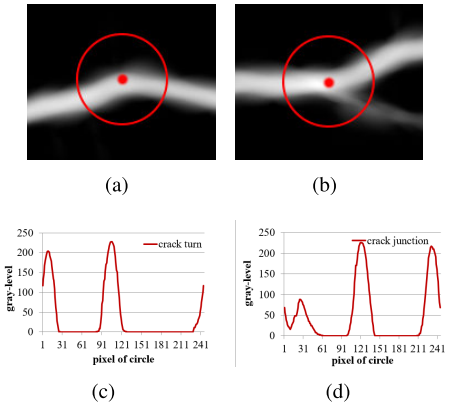

FIGURE 14. Analysis of the number of stick tensor peaks. (a) Stick tensor saliency of crack turn, (b) stick tensor saliency of crack junction, (c) values of Stick tensor saliency of pixels on the circle of (a), (d) values of stick tensor saliency of pixels on the circle of (b).

III. EXPERIMENTAL RESULTS

To test the proposed method, a diverse set of asphalt pavement images with various lighting condition are acquired using unmanned aerial vehicles. They are collected on the highway G45 in China with the image size of 2048 × 1536 pixels. 1 pixel represents a 2 mm × 2 mm area of the pavement surface according to the camera calibration parameters and aerial altitude of UAV. They involve lots of interferences on the pavement, like dirt debris, shadow, lane marking, etc. Among them, there are different type and size of crack junctions that are formed by different type of cracks, such as alligator crack, longitudinal crack, transverse crack, etc. Meanwhile, some typical concrete crack junction images collected from SDNET2018 data set [47] are also applied to evaluate the applicability of the proposed method. SDNET2018 is a public image data set with concrete bridge decks, walls, and pavements. It also includes different interferences, such as shadows, crack-like edges, and background debris.

For the parameter setting, in pavement image denoising, σ_d and σ_r are set as 2 and 35 according to the size of stone mixture and the gray-level difference between the crack and the pavement, respectively. In pavement image enhancement, the size of median filter window is set as 51 × 51 according to the width of large interferences, e.g., lane marking, in the pavement image. In correlation structure analysis, the size of correlation window is set as 5 × 5 according to the width of the hair-line crack. For iterative tensor voting, σ is set as 25, which can ensure that breaking segments are connected naturally without too much cost of computation time. The number of iterations N_{iter} is set as 2 according to the salience of crack junction candidate and the effect of noise in the stick tensor image. The radius of circle for crack junction detection with stick tensor saliency is set as 15 pixels.

A. CRACK JUNCTIONS OF DIFFERENT TYPE AND SIZE

As shown in Figure 15(a), some detection results of crack junctions of different type, including the $'X-','Y-','T-'$ shaped branching or crossing, are illustrated. These crack junctions are detected well by our method. Although the number of neighbouring crack curves around crack junctions is different, there is a generic characteristic of crack junction:

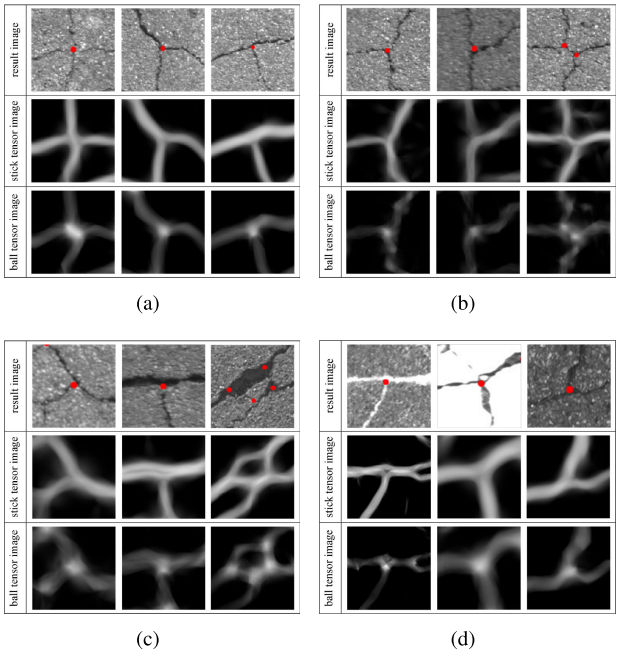

FIGURE 15. Detection results of crack junction. (a) Crack junctions of different type, (b) crack junctions with different orientation of crack curve, (c) crack junctions of different size, (d) special crack junctions. Detection results are marked with red points.

at least two main curves cross around the crack junction and the crack junction is a ball-like structure as shown in the stick tensor images and ball tensor images, respectively. The ball tensor characterization of crack junction is based on this generic characteristic. So, crack junction of different type can be extracted by our method in a unified framework.

In Figure 15(b), these crack junctions have the same type, but the orientations of neighbouring crack curves around crack junctions are different. The orientation of crack curves is arbitrary in the pavement image. It is difficult to characterize crack junctions by a template-based method. However, due to the unified ball-like structure characterization of crack junction, they are detected well by the ball tensor saliency.

The size of crack junctions varies a lot as shown in Figure 15(c). Although the width of crack curves is various, they show the same linear structure characteristic. The crack curves of different size are kept entirely after correlation structure analysis. So, crack junction of different size can get enough structure indications from their neighbouring crack curves and detected well by the proposed method as shown in the stick tensor images and ball tensor images.

Some special crack junctions are shown in Figure 15(d). They are with white filler, located on lane marking, and repaired. The proposed method is based on the structure characterization, not on the intensity threshold decomposition. Although the intensity of crack curves and pavement background are various, the significant ball-like structure of crack junctions is the same and well detected by the proposed tensor characterization from the structure perspective as shown in the ball tensor images.

Therefore, the proposed method for crack junction detection is independent of the type and size of junctions, and robust to the variance of the location, orientation and width of neighboring crack curves around crack junctions.

B. CRACK JUNCTIONS OF BREAKING SEGMENTS

As shown in rectangle of Figure 16(a) and 16(b), there is a obvious gap between the breaking segment and the crack junction due to physical breakup. Using the iterative tensor voting, this gap obtains the structure indications from the neighboring crack curves gradually and the breaking segment is connected naturally to the crack junction in Figure 16(c) and 16(d). The crack junction can then be located accurately as shown in Figure 16(e) and 16(f). Similarly, as shown in yellow rectangle of the first column of Figure 17, the breaking segments in enhanced image and correlation structure index image are linked well in the iterative tensor voting image. Crack junctions are located accurately in ball tensor image. Therefore, our method can fill gaps naturally and extract the unobvious crack junction.

C. CRACK JUNCTIONS WITH DIFFERENT INTERFERENCES AND IMAGING CONDITIONS

To obtain the hair-line crack curves, some stone mixtures are mistakenly extracted in enhanced image and correlation structure index image owing to the linear structure of

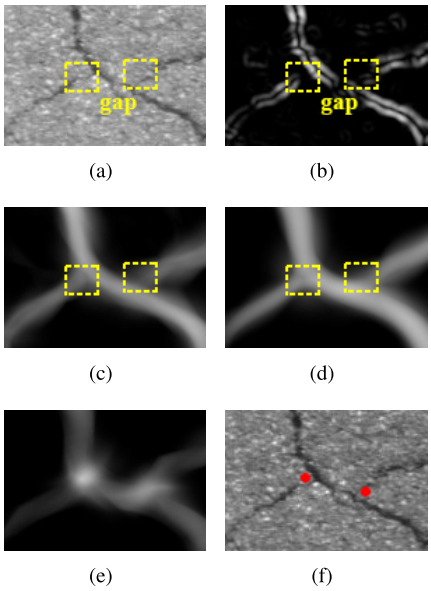

FIGURE 16. An illustration of the impact of breaking segments. (a) Original image, (b) correlation structure index image, (c) stick tensor image after first voting, (d) stick tensor image after second voting, (e) ball tensor image, (f) result of crack junction detection.

edge, as shown with the green ellipse of the first column of Figure 17. With the iterative tensor voting, the crack curves obtain more structure indications than the remaining stone mixtures due to less linear structures around stone mixture. These stone mixtures are eliminated well after the first tensor voting and cannot impact the final detection results.

Similarly, the dirt debris is mistakenly extracted as shown in the second column of Figure 17. Through iterative tensor voting, the dirt debris is weakened due to the absence of strong indications of crack-like structure in their neighborhood as shown in the iterative tensor voting image of Figure 16. Based on the local maximum of ball tensor, the dirt debris cannot be mistakenly detected by our method.

As shown in third column of Figure 17, some intersections of the crack and the edges of large interferences are marked with green ellipse. These junction-like structures interfere the crack junction detection seriously. They can be removed by the pavement image enhancement and correlation structure analysis. Meanwhile, both the crack junction located on the lane marking and crack junctions located on pavement are detected well by our method. Figure 18 shows the crack detection results with the interference of lane marking. Without median filter, lane marking cannot be removed from the pavement image and the junction-like structures caused by the lane marking edge and crack are mistakenly detected as shown in the yellow rectangles in Figure 18(b) and (d). Using the median filter, these large interferences can be removed from the pavement images and cannot mislead crack junction detection as shown in Figure 18(a) and (c).

Another important factor impacting crack junction detection is the imaging condition, which influences the contrast between the crack and the pavement and aggravates

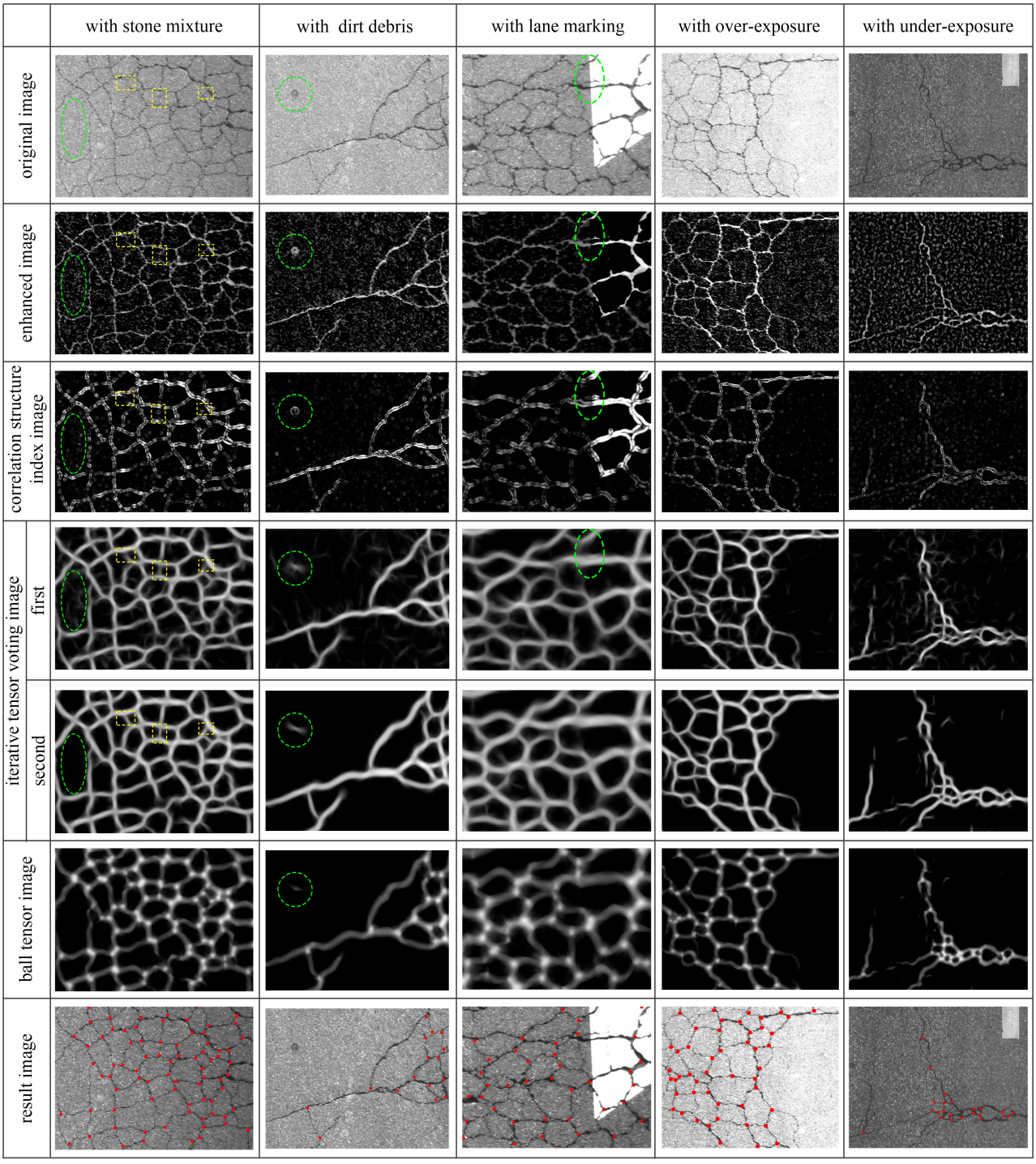

FIGURE 17. Results of our proposed method for crack junction detection with different interferences and imaging conditions.

the difficulty for crack junction detection. As shown in fourth and fifth column of Figure 17, the pavement images are over-expose and under-exposed, respectively. Comparing with the ordinary pavement image, they have more noise. Using the pavement image enhancement method, the contrast is improved significantly as shown in the enhancement image. Meanwhile, lots of noise introduced by the poor imaging condition is further eliminated by the correlation structure analysis. Crack junctions under poor imaging conditions are detected well as the same as the ordinary pavement image.

Therefore, the proposed method is robust enough to get a good detection result regardless of the pavement interferences and imaging conditions.

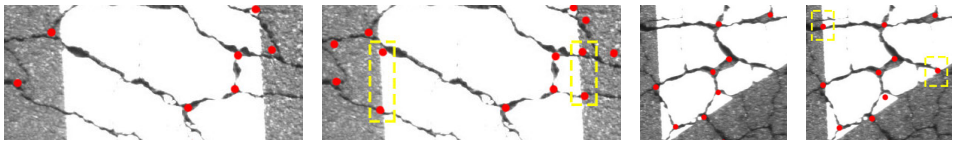

FIGURE 18. Crack detection results with the impact of lane marking. (a)(c) Using median filter, (b)(d) not using median filter.

D. EVALUATION OF CRACK JUNCTION DETECTION

To test the detection accuracy of the proposed method, the ground-truth location of crack junction is marked elaborately by the operators of transportation agencies. To avoid the subjectivity of manual marking, the morphological dilation with the circular structure element of 10-pixel radius is made to encircle the ground-truth crack junction. The size of structure element is set according to the minimal size of crack junction and the image size. If the detected crack junction falls inside the buffered ground truth, the detection result is true; otherwise, the detection result is false. The measure of correctness and completeness is adopted here to evaluate the detection accuracy of the proposed method. They can be calculated by the following equation:

$$correctness = \frac{T}{N_d} \tag{16}$$

$$completeness = \frac{T}{N_t} \tag{17}$$

where T is the number of crack junctions detected correctly by our method; N_d is the total number of junctions extracted by our method and N_t is the total number of crack junctions marked in the ground truth image.

Currently, there is no specific method for pavement crack junction detection. Therefore, a combined method of crack centerline detection and junction extraction is adopted to compare with the proposed method. B-COSFIRE (bar-selective combination of shifted filter responses) is used to extract the crack centerline [48]. B-COSFIRE can be applied in any computer vision methodology which requires the delineation of curvilinear. It also achieves state-of-the-art results for crack centerline detection in pavement images [49]. Then the crack junction candidates are detected by the crossing of skeletal centerline. To differentiate from the turn of crack curve, the number of crack centerlines around the junction is applied to get the final junctions from the candidates.

Sixteen concrete pavement images of SDNET2018 data set are selected and classified into four categories: common, with hair-line crack, with more noise and under-exposed, according to the crack junction characteristics and image conditions. Since the number of crack junction in single concrete image is small, the correctness and completeness of concrete crack junction are calculated according to the category of junction. Meanwhile, At the same time, sixteen typical asphalt pavement images are selected, which were classified into two categories according to the crack type: asphalt transverse/longitudinal crack junctions and asphalt alligator crack junctions. Then, based on crack junction characteristics, these images are divided into five categories: common, with hair-line crack, with interferences, with white filler and with more noise, The correctness and completeness of each image are calculated separately.

Detection results of some typical concrete pavement images are listed in the first part of Table 2 and shown in Figure 19. For the common images, the contrast between pavement and crack junction is high and the crack curve is smooth. The detection accuracy of the proposed method and B-COSFIRE is similar. For pavement image with hair-line crack, due to the influence of breaking segment of crack centerline, some junctions can not be detected well by B-COSFIRE with the correctness of 0.750 and completeness of 0.545. Comparing with the proposed method, the hair-line crack gets the structure indications from the neighboring crack curves and connects naturally to the crack junction as shown in Figure 19 (b). The average correctness and completeness of hair-line crack images are 0.900 and 0.818, respectively. For the pavement image with more noise and interferences as shown in Figure 19 (c), lots of crack-like structures are extracted into the crack centerline, which greatly increases the number of false junctions. The completeness and correctness of B-COSFIRE are 0.364 and 0.800. Moreover, when the contrast between pavement and crack is low, complete crack centerlines cannot be extracted correctly by B-COSFIRE. The correctness is 0.600 and completeness is 0.750 in Figure 19 (d). Due to the effect of pavement image enhancement and iterative structure propagation, our method has better robustness and applicability, and the completeness is above 0.800, regardless of the influence of noises, interferences and image conditions. The average correctness and completeness of concrete crack junction detection of B-COSFIRE method are 0.629 and 0.724. The average correctness and completeness of concrete crack junction detection of the proposed method are 0.889 and 0.842.

The second part of Table 2 shows the detection result of asphalt transverse/longitudinal crack junctions. Some local detection results of the proposed method and B-COSFIRE are shown in Figure 20 (a) and the detection results of the whole image are shown in Figure 21. The detection result of transverse or longitudinal crack junctions is similar with that of concrete crack junction. For common images, the number of crack junction is small and the detection correctness

TABLE 2. The correctness and completeness of some typical crack junction images.

crack type		image	correctness		completeness	
			our method	B-COSFIRE	our method	B-COSFIRE
concrete crack junction	common	-	1	0.800	1	0.800
	with hair-line crack	-	0.900	0.750	0.818	0.545
	with more noise	-	0.800	0.364	0.800	0.800
	under-exposed	-	0.857	0.600	0.750	0.750
	mean		0.889	0.629	0.842	0.724
asphalt transverse/longitudinal cracks	common	SXX__2546	1	1	1	1
		SXX__3543	1	1	1	1
	with hair-line crack	SXX__3544	1	0.500	0.909	0.7271
		SXX__3551	0.813	0.594	0.765	0.765
	with interferences	SXX__3575	0.708	0.438	0.739	0.435
		SXX__5072	1	0.500	1	0.500
	with white filler	SXX__9051	0.895	0.458	0.810	0.579
	with more noise	SXX__5184	0.900	0.429	0.750	0.500
	mean		0.915	0.615	0.872	0.688
asphalt alligator crack	common	SXX__3539	0.923	0.570	0.944	0.665
		SXX__3542	0.853	0.480	0.926	0.677
	with hair-line crack	SXX__3554	0.835	0.697	0.901	0.447
		SXX__3541	0.896	0.504	0.890	0.790
	with interferences	SXX__3560	0.839	0.738	0.906	0.447
		SXX__3548	0.874	0.644	0.891	0.410
	with white filler	SXX__9069	0.832	0.831	0.915	0.731
	with more noise	SXX__4226	0.885	0.037	0.852	0.026
	mean		0.867	0.562	0.903	0.524
MEAN			0.891	0.597	0.887	0.630

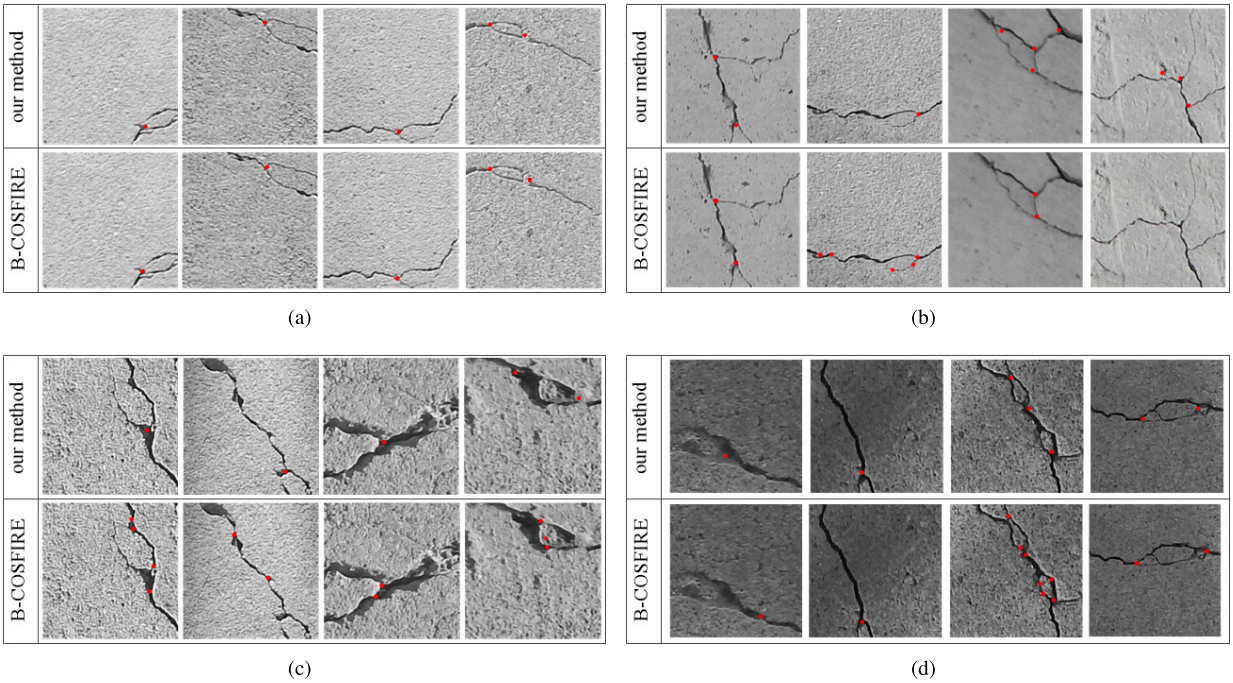

FIGURE 19. An illustration of detection results of typical concrete crack images. (a) Common, (b) with hair-line crack, (c) with more noise, (d) under-exposed. Detection results are marked with red points.

and completeness are almost 1 for both our method and B-COSFIRE. For pavement image with hair-line crack, some crack junctions cannot be detected by B-COSFIRE as shown in second part of Figure 20 (a). For the pavement images with more noise, the correctness is 0.429 and completeness is 0.500 for B-COSFIRE. Based on iterative the structure propagation, the breaking segments are connected and the noise is removed gradually. Therefore, both correctness and

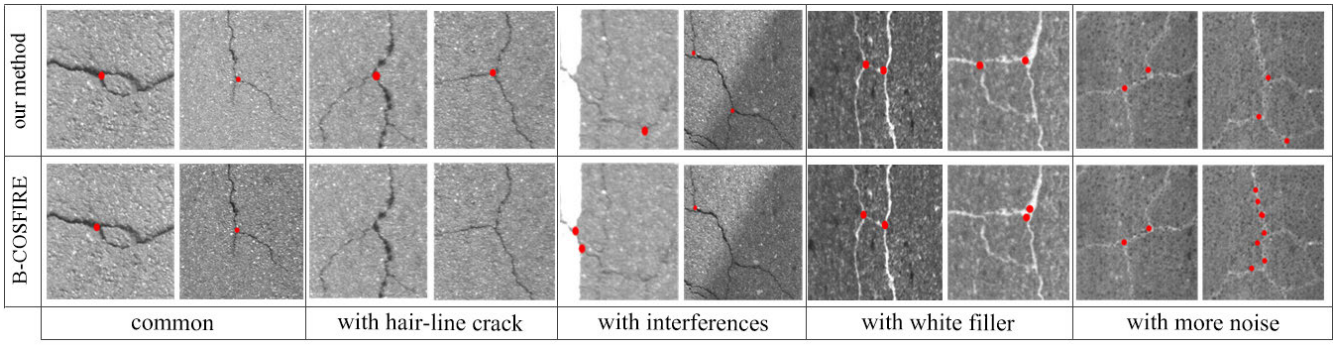

(a)

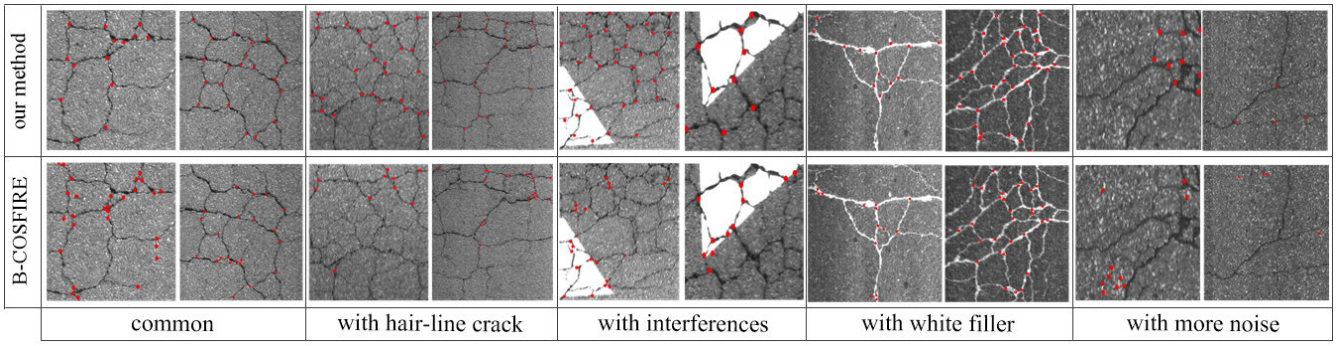

(b)

FIGURE 20. An illustration of detection results of typical asphalt crack images. (a) Transverse/Longitudinal cracks, (b) Alligator crack. Detection results are marked with red points.

completeness of the proposed method are better than 0.700. Moreover, the junction-like structures formed at the intersection of the crack and the lane marking edge are mistakenly extracted by the B-COSFIRE as shown in third part of 20 (a). However, these large interferences cannot influence the detection result of the proposed method. The average correctness and completeness of asphalt transverse/longitudinal crack junction detection of B-COSFIRE are 0.615 and 0.688. The average correctness and completeness of our method are 0.915 and 0.872. Results of junction detection is helpful to tell the change of severity level for the accurate location of branching in the transverse or longitudinal cracking.

The third parts of Table 2 and Figure 20 (b) show the detection result of asphalt alligator crack junctions. Differently, for one alligator crack image, crack junctions have different type, size and intensity and the contrast between pavement and crack junction varies a lot. It is difficult for B-COSFIRE method to completely extract the centerlines of the wide and hair-line cracks with no additional false junction-like structures as shown in 20 (b). In our method, using iterative structure propagation, both wide cracks and hair-line cracks can get enough indications to extract crack junctions. Meanwhile, the additional false junction-like structures can be removed gradually due to the less structural indications. For the common image of SXX_3539, the detection correctness and completeness of our method are 0.923 and 0.944, respectively, which are superior to the detection result of B-COSFIRE method with the correctness of 0.570 and completeness of 0.655. For the more noisy image of SXX_4226, the correctness and completeness of B-COSFIRE are as low as 0.037 and 0.026, respectively, which is affected by the noise interferences and low contrast in the pavement image. In this case, our method can still detect well with the correctness of 0.855 and completeness of 0.852 as shown in the final image in 20 (b). The average correctness and completeness of asphalt alligator crack junction detection of B-COSFIRE are reduced to 0.562 and 0.524. The average correctness and completeness of our method are 0.867 and 0.903. The accurate extraction of alligator crack junctions provides a reliable indication to quantify the severity level of alligator cracks.

Therefore, the results demonstrate that the proposed method can detect crack junctions with the correctness of 0.891 and completeness of 0.887. The average correctness and completeness of B-COSFIRE method are 0.597 and 0.630, respectively. It demonstrates the proposed method can be applied to junction detection on concrete pavement and alligator pavement images. It can extract more complete crack junctions with high accuracy, especially for the alligator crack junctions. Moreover, the proposed method has better robustness to different noise and interference.

IV. DISCUSSIONS

In our method, there are two important parameters, which influence the result of crack junction detection. To make the proposed method applicable for different pavement images and get a good result, we discuss the parameter setting here.

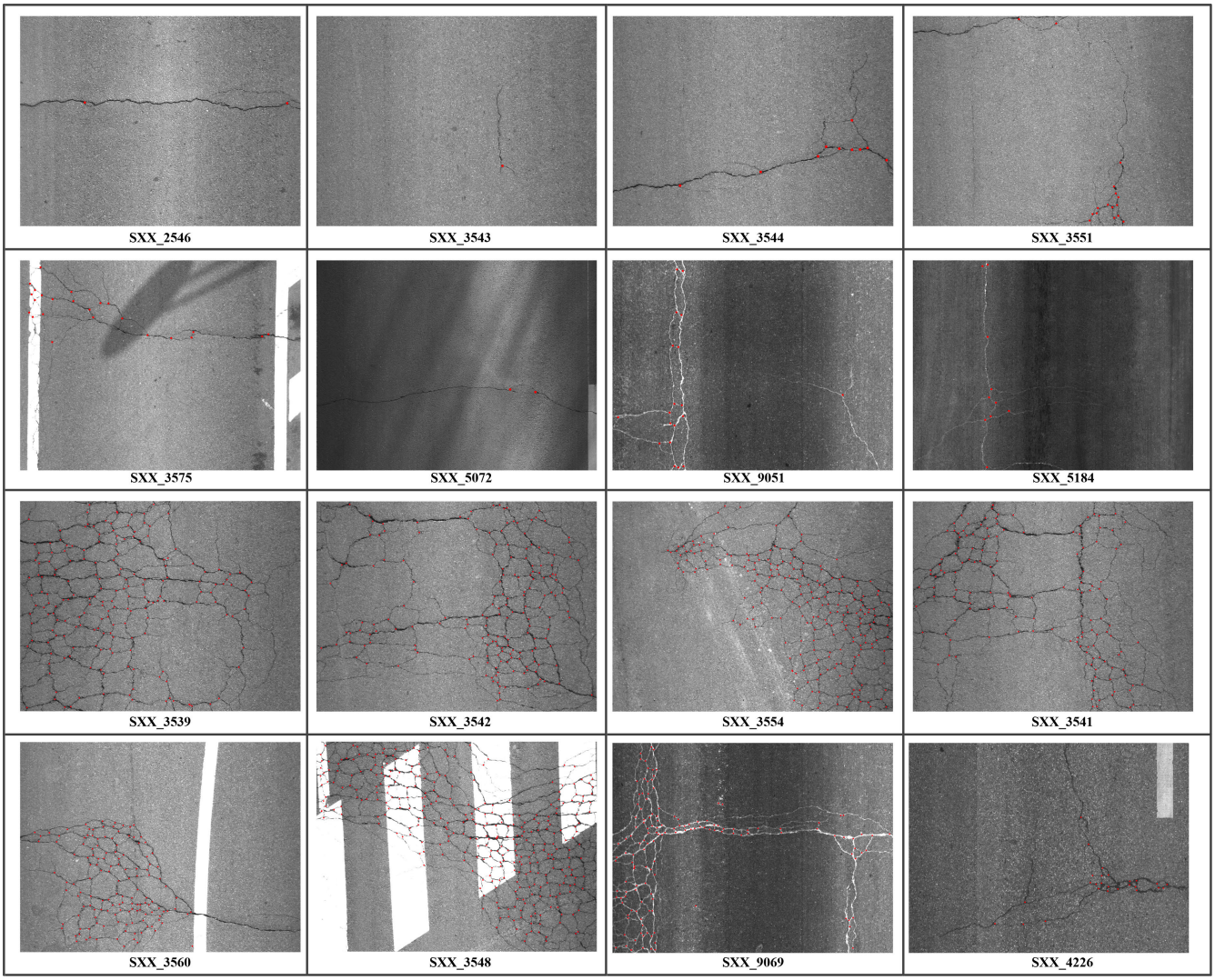

FIGURE 21. An illustration of detection results of typical crack images. Detection results are marked with red points.

A. SIZE OF LOCAL PATCH OF CORRELATION STRUCTURE ANALYSIS

The only and most important parameter of the correlation analysis is the size of local patch in correlation structure analysis. If the local patch is small, some small stone mixture will be mistakenly extracted as crack junction candidates. Correlation structure analysis with a large local patch can remove the ball-like structures, like stone mixture, owing to the anisotropy of gradients. But crack curves of small width, like hair-line cracks, are unexpectedly discard due to the weaker crack-like structure in a larger patch. Therefore, to keep the entire crack curves robustly, size of local patch is set to according to the width of crack in the pavement image.

As shown in 22(a), there is a hair-line crack in the pavement image and size of local patch is decided on it. For a 7×7 window as shown in Figure 22(a), there is an obvious linear structure. However, lots of pavement pixels also exists in this local patch. It weakens the characteristic of correlation structure analysis as shown in Figure 22(b). For correlation

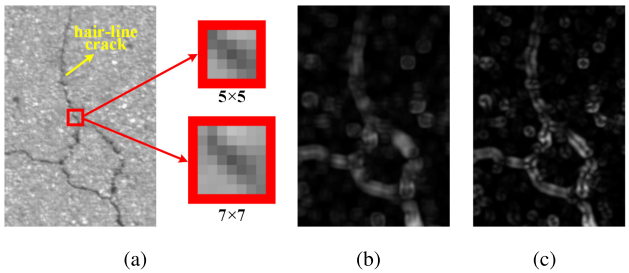

FIGURE 22. Local patch selection of correlation structure analysis. (a) Hair-line crack and size of local patch, (b) correlation structure index with a local patch of 7×7 pixels, (c) correlation structure index with a local patch of 5×5 pixels.

structure analysis with a 5×5 window in Figure 22(c), structure of hair-line crack is more obvious than that with a 7×7 window, which helps get a more complete set of crack junction candidate. Hence, we set the size of local patch equals 5×5. In our method, the hair-line crack can be seen as a reference to set the size of local patch in correlation structure analysis.

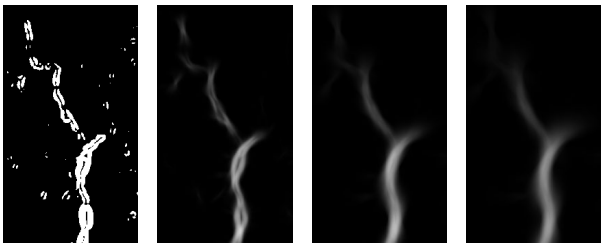

FIGURE 23. Scale parameter setting in tensor voting. (a) Crack junction candidate, (b-d) Tensor voting with σ= 12.5, 25, 35, respectively.

B. SCALE PARAMETER OF ITERATIVE TENSOR VOTING

In iterative tensor voting, the scale parameter σ controls the size of voting field. To connect the breaking segments to crack junctions, the voting fields should at least cover the gaps between the breaking segments and the crack junctions. Additionally, due to the effects of saliency decay function, σ is set twice the value that are calculated from the distance between breaking segments based on equation 13 to get enough structure indications for the gaps.

As shown in Figure 23(a), there are many gaps among breaking segments. The size of gap is about 21 pixels. When σ equals 12.5, semi-width of the voting filed is then 27 pixels by equation 13, which can fill the gaps. However, breaking segments are not connected well in Figure 23(b) due to the insufficient structure indications. As shown in Figure 23(c), when σ equals 25, the breaking segments are connected naturally. However, when σ equals 35 in Figure 23(d), the result of tensor voting is identical to the result of Figure 23(c). But the computation time increases greatly. Therefore, σ should ensure that breaking segments are connected naturally without too much cost of computation time. In our method, the value of σ is 25.

V. CONCLUSION

Crack junction is the crossing or branching point of different cracks. It represents the branch of transverse crack or longitudinal crack. The interlaced network of alligator crack is indicated by junctions. It is simple yet important factor in crack semantic structure extraction, classification, severity level quantification. This paper is dedicated to detect crack junction in the pavement image for the first time.

The proposed method is based on the structure characterization of crack junction that is generic and robust to different imaging conditions. The pavement image is enhanced by denoising and removing large interferences. Based on the correlation structure analysis, candidates of crack junction are extracted by the proposed correlation structure index. Ball tensor is employed to characterize the candidates of different type and size in a unified framework. Using the iterative tensor voting, crack junction structure is enhanced and some interferences, such as stone mixture and dirt debris, are gradually eliminated. Actual junctions are identified among the candidates by with the saliency of ball tensor and the linear structure surrounding them.

The proposed method achieves high correctness of 0.891 and completeness of 0.887. It demonstrates the proposed method can be applied to junction detection on both concrete and asphalt pavement images. Meanwhile, the proposed method for crack junction detection is independent of the type and size of junctions, and is robust for different interferences and imaging conditions. The unobvious crack junction causing by the physical breakup of faint crack or poor imaging condition can be well detected by our method. In the future research, we will test the proposed method with more crack image data sets and develop the method for crack classification and severity level estimation based on the density and distribution of crack junctions.

ACKNOWLEDGMENT

The authors would like to thank the editors and anonymous reviewers for their valuable comments, which helped improve this article.

REFERENCES

[1] S. Dorafshan, R. J. Thomas, and M. Maguire, "Comparison of deep convolutional neural networks and edge detectors for image-based crack detection in concrete," *Construct. Building Mater.*, vol. 186, pp. 1031–1045, Oct. 2018.
[2] N.-D. Hoang, "Automatic detection of asphalt pavement raveling using image texture based feature extraction and stochastic gradient descent logistic regression," *Autom. Construct.*, vol. 105, Sep. 2019, Art. no. 102843.
[3] *Standard Practice for Quantifying Cracks in Asphalt Pavement Surface*, Assoc. State Highway Transp. Officials, Washington, DC, USA, 2001.
[4] *Standard Practice for Quantifying Cracks in Asphalt Pavement Surfaces from Collected Images Utilizing Automated Methods*. Assoc. State Highway Transp. Officials, Washington, DC, USA, 2003.
[5] *Distress Identification Manual for the Long-Term Pavement Performance Program*, Federal Highway Admin., Washington, DC, USA, 2003.
[6] P. Fu, J. T. Harvey, J. N. Lee, and P. Vacura, "New method for classifying and quantifying cracking of flexible pavements in automated pavement condition survey," *Transp. Res. Rec., J. Transp. Res. Board*, vol. 2225, no. 1, pp. 99–108, Jan. 2011.
[7] S. Qiu, W. Wang, S. Wang, and K. C. Wang, "Methodology for accurate AASHTO PP67-10–based cracking quantification using 1-mm 3D pavement images," *J. Comput. Civil Eng.*, vol. 31, no. 2, Mar. 2016, Art. no. 4016056.
[8] *Flexible Pavement Condition Survey Handbook*, State Mater. Office, Davie, FL, USA, 2009.
[9] *Pavement Management Information System Rater's Manual*, Texas Dept. Transp., Austin, TX, USA, 2010.
[10] S. Li, Y. Cao, and H. Cai, "Automatic pavement-crack detection and segmentation based on steerable matched filtering and an active contour model," *J. Comput. Civil Eng.*, vol. 31, no. 5, Sep. 2017, Art. no. 4017045.
[11] Y. Tsai, C. Jiang, and Y. Huang, "Multiscale crack fundamental element model for real-world pavement crack classification," *J. Comput. Civil Eng.*, vol. 28, no. 4, Jul. 2014, Art. no. 4014012.
[12] B. Wang, W. Zhao, P. Gao, Y. Zhang, and Z. Wang, "Crack damage detection method via multiple visual features and efficient multi-task learning model," *Sensors*, vol. 18, no. 6, p. 1796, Jun. 2018.
[13] S. Ghanta, S. S. Shamsabadi, J. Dy, M. Wang, and R. Birken, "A hessian-based methodology for automatic surface crack detection and classification from pavement images," *Proc. SPIE*, vol. 9437, Apr. 2015, Art. no. 94371Z.
[14] A. Arena, C. D. Piane, and J. Sarout, "A new computational approach to cracks quantification from 2D image analysis: Application to micro-cracks description in rocks," *Comput. Geosci.*, vol. 66, pp. 106–120, May 2014.
[15] Z. Qu, Y.-X. Chen, L. Liu, Y. Xie, and Q. Zhou, "The algorithm of concrete surface crack detection based on the genetic programming and percolation model," *IEEE Access*, vol. 7, pp. 57592–57603, 2019.

[16] C. Jiang, "A crack detection and diagnosis methodology for automated pavement condition evaluation," Ph.D. dissertation, Georgia Inst. Technol., Atlanta, GA, USA, 2015.
[17] R. Li, Y. Yuan, W. Zhang, and Y. Yuan, "Unified vision-based methodology for simultaneous concrete defect detection and geolocalization," *Comput. Aided Civil Infrastruct. Eng.*, vol. 33, no. 7, pp. 527–544, Jul. 2018.
[18] B. Kim and S. Cho, "Automated vision-based detection of cracks on concrete surfaces using a deep learning technique," *Sensors*, vol. 18, no. 10, p. 3452, Oct. 2018.
[19] Y. Li, H. Li, and H. Wang, "Pixel-wise crack detection using deep local pattern predictor for robot application," *Sensors*, vol. 18, no. 9, p. 3042, Sep. 2018.
[20] W. Wu, M. A. Qurishee, J. Owino, I. Fomunung, M. Onyango, and B. Atolagbe, "Coupling deep learning and UAV for infrastructure condition assessment automation," in *Proc. IEEE Int. Smart Cities Conf. (ISC)*, Sep. 2018. pp. 1–7.
[21] S. Bang, S. Park, H. Kim, and H. Kim, "Encoder–decoder network for pixel-level road crack detection in black-box images," *Comput.-Aided Civil Infrastruct. Eng.*, vol. 34, no. 8, pp. 713–727, Aug. 2019.
[22] Y.-J. Cha, W. Choi, and O. Büyüköztürk, "Deep learning-based crack damage detection using convolutional neural networks," *Comput.-Aided Civil Infrastruct. Eng.*, vol. 32, no. 5, pp. 361–378, May 2017.
[23] X. Yang, H. Li, Y. Yu, X. Luo, T. Huang, and X. Yang, "Automatic pixel-level crack detection and measurement using fully convolutional network," *Comput.-Aided Civil Infrastruct. Eng.*, vol. 33, no. 12, pp. 1090–1109, Dec. 2018.
[24] E. Zalama, J. Gómez-García-Bermejo, R. Medina, and J. Llamas, "Road crack detection using visual features extracted by Gabor filters," *Comput.-Aided Civil Infrastruct. Eng.*, vol. 29, no. 5, pp. 342–358, May 2014.
[25] N.-D. Hoang, Q.-L. Nguyen, and D. T. Bui, "Image processing–based classification of asphalt pavement cracks using support vector machine optimized by artificial bee colony," *J. Comput. Civil Eng.*, vol. 32, no. 5, Sep. 2018, Art. no. 4018037.
[26] A. Zhang, K. C. P. Wang, Y. Fei, Y. Liu, C. Chen, G. Yang, J. Q. Li, E. Yang, and S. Qiu, "Automated pixel-level pavement crack detection on 3D asphalt surfaces with a recurrent neural network," *Comput.-Aided Civil Infrastruct. Eng.*, vol. 34, no. 3, pp. 213–229, Mar. 2019.
[27] R. Elias and A. Elnahas, "An accurate indoor localization technique using image matching," in *Proc. 3rd IET Int. Conf. Intell. Environ.*, Sep. 2007, pp. 376–382.
[28] S. Kamel, M. Moharram, and R. Elias, "Wide baseline stereo matching through junction parametric and polar warping," in *Proc. Int. Conf. Comput. Graph. Imag.*, 2010, pp. 59–64.
[29] C.-L. Tsai, C. V. Stewart, H. L. Tanenbaum, and B. Roysam, "Model-based method for improving the accuracy and repeatability of estimating vascular bifurcations and crossovers from retinal fundus images," *IEEE Trans. Inf. Technol. Biomed.*, vol. 8, no. 2, pp. 122–130, Jun. 2004.
[30] S. H. Wiering and L. Schomaker, "Junction detection in handwritten documents and its application to writer identification," *Pattern Recognit.*, vol. 48, no. 12, pp. 4036–4048, Dec. 2015.
[31] G.-S. Xia, J. Delon, and Y. Gousseau, "Accurate junction detection and characterization in natural images," *Int. J. Comput. Vis.*, vol. 106, no. 1, pp. 31–56, Jan. 2014.
[32] T. Luo, J. Zhang, and L. Lian, "Speed up junction detector based on azimuth consensus by Harris corner," *Opt. Rev.*, vol. 21, no. 2, pp. 135–142, Mar. 2014.
[33] R. Elias and R. Laganière, "Judoca: Junction detection operator based on circumferential anchors," *IEEE Trans. Image Process.*, vol. 21, no. 4, pp. 2109–2118, Apr. 2012.
[34] T.-A. Pham, M. Delalandre, S. Barrat, and J.-Y. Ramel, "Accurate junction detection and characterization in line-drawing images," *Pattern Recognit.*, vol. 47, no. 1, pp. 282–295, 2014.
[35] Z. Tu and X. Chen, "Junction detection based on line segments," in *Proc. 9th IEEE Conf. Ind. Electron. Appl.*, Jun. 2014, pp. 1231–1234.
[36] S. Abbasi-Sureshjani, I. Smit-Ockeloen, E. Bekkers, B. Dashtbozorg, and B. Romeny, "Automatic detection of vascular bifurcations and crossings in retinal images using orientation scores," in *Proc. IEEE 13th Int. Symp. Biomed. Imag. (ISBI)*, Apr. 2016, pp. 189–192.
[37] R. Su, C. Sun, and T. D. Pham, "Junction detection for linear structures based on Hessian, correlation and shape information," *Pattern Recognit.*, vol. 45, no. 10, pp. 3695–3706, Oct. 2012.
[38] E. D. Sinzinger, "A model-based approach to junction detection using radial energy," *Pattern Recognit.*, vol. 41, no. 2, pp. 494–505, Feb. 2008.
[39] G.-S. Xia, J. Delon, and Y. Gousseau, "An accurate and contrast invariant junction detector," in *Proc. 21st Int. Conf. Pattern Recognit. (ICPR)*, Nov. 2012, pp. 2780–2783.
[40] C. Tomasi and R. Manduchi, "Bilateral filtering for gray and color images," in *Proc. 6th Int. Conf. Comput. Vis.*, Jan. 1998, pp. 839–846.
[41] J. Astola and P. Kuosmanen, *Fundamentals of Nonlinear Digital Filtering*. Boca Raton, FL, USA: CRC Press, 1997.
[42] G. Agam, S. G. Armato, and C. Wu, "Vessel tree reconstruction in thoracic CT scans with application to nodule detection," *IEEE Trans. Med. Imag.*, vol. 24, no. 4, pp. 486–499, Apr. 2005.
[43] G. Medioni and S. B. Kang, *Merging Topics in Computer Vision*. Upper Saddle River, NJ, USA: Prentice-Hall, 2004.
[44] G. Guy, "Inference of multiple curves and surfaces from sparse data," Univ. Southern California, Los Angeles, CA, USA, Tech. Rep. 96-345, 1997.
[45] G. Guy and G. Medioni, "Inferring global perceptual contours from local features," in *Proc. IEEE Conf. Comput. Vis. Pattern Recognit.*, Jun. 1993, pp. 786–787.
[46] L. Loss, G. Bebis, M. Nicolescu, and A. Skurikhin, "An iterative multi-scale tensor voting scheme for perceptual grouping of natural shapes in cluttered backgrounds," *Comput. Vis. Image Und.*, vol. 113, no. 1, pp. 126–149, Jan. 2009.
[47] S. Dorafshan, R. J. Thomas, and M. Maguire, "SDNET2018: An annotated image dataset for non-contact concrete crack detection using deep convolutional neural networks," *Data brief*, vol. 21, pp. 1664–1668, Dec. 2018.
[48] G. Azzopardi, N. Strisciuglio, M. Vento, and N. Petkov, "Trainable COSFIRE filters for vessel delineation with application to retinal images," *Med. Image Anal.*, vol. 19, no. 1, pp. 46–57, Jan. 2015.
[49] N. Strisciuglio, G. Azzopardi, and N. Petkov, "Detection of curved lines with B-COSFIRE filters: A case study on crack delineation," in *Computer Analysis of Images and Patterns* (Lecture Notes in Computer Science), vol. 10424. Cham, Switzerland: Springer, 2017, pp. 108–120.

YANLI WANG received the B.Sc. degree in surveying and mapping engineering from East China Jiaotong University, Nanchang, China, in 2015. She is currently pursuing the Ph.D. degree with Wuhan University.

Her current research interest includes the remote sensing image processing.

YUCHUN HUANG received the Ph.D. degree in information and communication engineering from the Huazhong University of Science and Technology, Wuhan, China. He is currently an Associate Professor with the School of Remote Sensing and Information Engineering, Wuhan University, China, where he serves as the Leader of Research Group on Mobile Mapping System. His research interests include pavement condition survey, data fusion of multiple sensors, image and LiDAR data processing, and intelligent and remote sensing systems on transportation.

WEIHONG HUANG received the B.Sc. degree in channel ports and coastal engineering and the master's degree in traffic engineering from Chongqing Communication University, Chongqing, China, in 2004 and 2015, respectively. He has been dedicated to the Condition Survey Practice and Planning in Chongqing, for several years. He is currently a Senior Engineer with Chongqing Communications Planning Survey and Design Institute, China. His current research interest includes the condition survey practice and planning.